Research Square

Preprints are preliminary reports that have not undergone peer review.
They should not be considered conclusive, used to inform clinical practice,
or referenced by the media as validated information.

An Automated QGIS Plugin to Generate ENVI-met Traffic Emission Sources from Vehicle Trajectories

Tim Sinsel

t.sinsel@geo.uni-mainz.de

Johannes Gutenberg University Mainz

Christian Fries

University of Münster

Pascal Lukas

Johannes Gutenberg University Mainz

Helge Simon

Johannes Gutenberg University Mainz

Peer Schöneberger

Johannes Gutenberg University Mainz

Michael Bruse

Johannes Gutenberg University Mainz

Method Article

Keywords: Microclimate modeling, SUMO, Urban air quality, Background concentration forcing, Local concentration increment, LaStTraM footprint analysis

Posted Date: November 17th, 2026

DOI: https://doi.org/10.21203/rs.3.rs-11389285/v1

License: This work is licensed under a Creative Commons Attribution 4.0 International License.
Read Full License

Additional Declarations: Competing interest reported. T. Sinsel and H. Simon act as part-time freelance consultants and software developers for One Click LCA, the company that commercializes the ENVI-met software used in this study.

An Automated QGIS Plugin to Generate ENVI-met Traffic Emission Sources from Vehicle Trajectories

Authors

Tim Sinsel [a,*]; Christian Fries [b]; Pascal Lukas [a]; Helge Simon [a]; Peer Schöneberger [a]; Michael Bruse [a]

Affiliation

[a] Department of Geography, Johannes Gutenberg University Mainz, 55099 Mainz, Germany

[b] Institute for Geoinformatics, University of Münster, 48149 Münster, Germany

* Corresponding author. E-mail address: t.sinsel@geo.uni-mainz.de

Abstract

Traffic-related particulate matter (PM) and nitrogen oxides (NOx) are critical urban health risks. Microclimate models such as ENVI-met can resolve their street-level distribution, but feeding them with traffic data remains a manual bottleneck, so modelers generalize traffic into polygons or uniform line sources. This study presents an automated method, implemented as an open-source QGIS plugin, that converts vehicle trajectories into street-segment-specific ENVI-met line sources with hourly emission profiles. The plugin discretizes the road network, counts trips per segment, aligns trip times with the model clock, groups segments with similar traffic and splits NOx and PM emissions into the model species. To evaluate the generated sources, the background concentration forcing of ENVI-met V6 is combined with an evaluation of the local concentration increment and a backward Lagrangian footprint analysis, which separate the local traffic signal from the regional background and trace deviations from observations to their cause. Tested with SUMO-generated trajectories

at an official Berlin traffic station on six summer and autumn days, the method reproduced PM with high agreement (R^2 = 0.94 for PM2.5 and 0.82 for PM10), largely through the background, and 71 % of the measured local NOx increment with passenger-car trajectories alone. The footprint confirmed that this signal originates almost exclusively from the adjacent street canyon, and the remaining deviations were traced mainly to the vehicle classes missing from the demonstration dataset rather than to the gas-phase chemistry. By replacing manual data entry, the method provides segment-specific emission input for exposure assessments and planning scenarios.

Keywords

Microclimate modeling; SUMO; Urban air quality; Background concentration forcing; Local concentration increment; LaStTraM footprint analysis

1 Introduction

Ambient air pollution is globally recognized as one of the most severe environmental health risks, linked to cardiovascular and respiratory diseases that frequently result in premature mortality [1]. The physiological impact of pollutants is highly dependent on their characteristics, with particulate matter (PM), for example, being capable of penetrating deep into the bronchial system and triggering severe lung dysfunction [2–4]. Similarly, nitrogen oxides (NOx), specifically nitrogen dioxide (NO_2), pose a threat to public health and respiratory function, as the European Environment Agency estimated that 34,000 premature deaths across the EU in 2023 were attributable to ambient NO_2 exposure [5]. In urban areas, a persistent driver of this localized air pollution is vehicular traffic [6–8]. Because traffic-related air pollutants are emitted directly at street level, their dispersion is frequently impeded by urban morphologies and street canyon geometries, generating hotspots where concentrations substantially

exceed regional averages [9, 10]. To monitor these impacts and ensure compliance with regulatory thresholds, authorities rely on active measurement networks [11]. These stations provide indicators of current health risks. However, their deployment is sparse, and they cannot capture the heterogeneous spatial distribution of pollutants across an entire city grid [12]. Atmospheric modeling is hence required to fill these spatial gaps [13]. In addition, modeling provides predictive capabilities, allowing urban planners to simulate the potential effects of traffic interventions such as speed reductions, road closures, or toll implementations on both traffic flow and the subsequent distribution of air pollutants [14].

The atmospheric modeling landscape consists of various tools tailored to specific spatial scales. Regional chemical transport models are utilized to analyze large-scale advection processes, such as pollution originating from industrial facilities, distant construction sites, or natural phenomena like Sahara dust events, where synoptic weather patterns are the primary drivers [15–18]. Conversely, for specific microclimatic distribution analyses within the urban canopy, researchers increasingly rely on high-resolution, three-dimensional fluid dynamics models. Large-Eddy Simulation (LES) frameworks, such as PALM-4U, can provide highly accurate representations of these turbulent urban environments and hence air pollution distributions [19, 20]. However, the operational utility of LES is constrained by its computational requirements, typically necessitating high-performance supercomputers.

For standard desktop users, such as typical urban planners and environmental consultancies, the ENVI-met RANS model serves as an accessible and widely adopted alternative, as it balances necessary micro-scale spatial resolution with computational efficiency [21, 22]. Within the ENVI-met framework, the transport and dispersion of emitted pollutants from local sources are calculated using an Eulerian approach,

77 specifically by numerically solving the three-dimensional advection-diffusion equation.
78 This atmospheric chemistry and dispersion module is dynamically coupled to the
79 model's non-hydrostatic flow core, where the advection of pollutants is driven by the
80 resolved mean wind fields, while turbulent diffusion is parameterized utilizing the
81 standard $E-\varepsilon$ turbulence closure scheme [23]. Its air pollution module is
82 predominantly utilized to assess the efficacy of urban green infrastructure in mitigating
83 traffic-related PM, simulating how specific vegetation configurations, such as tree
84 morphologies, planting patterns, spacing, and tree-shrub combinations, alter local
85 aerodynamic flows and pollutant deposition within street canyons and parks [24–32].
86 Other exemplary use cases were related to BVOC and isoprene emission modelling or
87 vertical exposure differences for PM [33, 34]. When validated against empirical field
88 measurements, ENVI-met has proven capable of capturing horizontal and vertical
89 spatial concentration differences as well as the relative dispersion effects of varied
90 green space structures [29, 31]. However, performance evaluations of earlier model
91 versions highlight a tendency to underpredict absolute PM concentrations. This
92 tendency has been documented across multiple validation studies utilizing various
93 methods, including stationary monitoring, measurement campaigns, and biomagnetic
94 monitoring [35–38]. For example, a comparative evaluation utilizing an older model
95 version demonstrated that ENVI-met undercut predicted PM10 concentrations by a
96 factor of approximately two when benchmarked against established regulatory
97 Lagrangian models [37]. Crucially, these historical underpredictions can be directly
98 attributed to software limitations at the time: none of these earlier studies were able to
99 utilize dynamic background concentration forcing. Because the older model versions
100 lacked the capacity to incorporate larger-scale advection processes, the simulations

only accounted for localized emissions, inherently missing the regional baseline pollution that strongly affects onsite measurements.

The recently released ENVI-met Version 6 introduces a critical advancement by allowing the forcing of dynamic background concentrations [39], thereby addressing the primary driver of these historical underpredictions. Yet, while the model can now account for large-scale advection, a major methodological barrier persists regarding the local emissions themselves: accurately feeding the model with granular, street-segment-specific traffic data. Manually defining differing traffic volumes and emission profiles for individual streets or street-segments is practically unfeasible. Modelers need to generalize traffic networks into broad polygons or uniform line sources, degrading the precision of the underlying data and potentially introducing spatial allocation errors. Recent efforts have increasingly focused on coupling microscopic traffic and emission models with high-resolution CFD models to capture these granular dynamics. For example, integrated frameworks have been developed to link the SUMO traffic model with emission models like MOVES or EMIMO, which then feed into microscale CFD or 3D grid-based dispersion models [40, 41]. Other recent advancements include coupling the agent-based transport simulation MATSim with the LES model PALM-4U [19, 20], requiring map-matching procedures to project network links back onto real street geometries.

Background concentration forcing also changes how such simulations need to be evaluated. Once the regional background is prescribed, it dominates the modeled concentrations at a monitoring site, particularly for PM, so that the agreement of the total concentrations largely reflects the forcing rather than the simulated local processes. What a microscale model adds is the local concentration increment above the background. This increment varies within street canyons, differs between planning

scenarios, in which the background cancels out, and is thus the quantity that matters for local exposure assessments and urban planning. It also gains regulatory weight, as the revised EU Ambient Air Quality Directive lowers the annual limit values for PM2.5, PM10 and NO_2 to 10, 20 and 20 µg/m³ from 2030 [42], so that local increments of a few µg/m³ become relevant for compliance. Simulating this increment, however, requires a realistic, spatially explicit representation of the local traffic emissions.

To address the methodological gap of manual traffic data input, this study presents a novel workflow that utilizes explicit traffic trajectory data, derived either from field measurements or traffic models, to generate street-segment-specific ENVI-met emission sources. This automated process is easily accessible via a newly developed QGIS plugin (Traffic Data to ENVI-met) [43, 44]. By discretizing road networks and assigning dynamic emission fluxes to line-segments, this tool overcomes the traditional bottleneck of microclimate air pollution modeling. To demonstrate the reliability and practical application of this new workflow, we conduct proof-of-concept simulations for an urban street canyon in Berlin, Germany. Utilizing the QGIS plugin to parameterize the explicit vehicular sources, the simulations are tested against official in-situ measurements across six distinct days representing varying seasonal and meteorological situations (stable autumn and convective summer atmospheric conditions) to evaluate the novel modeling approach, with the local concentration increment above the forced background as the measure of the simulated traffic contribution.

2 Methodology

This section outlines the methodological framework applied to configure, execute, and evaluate the micro-scale air pollution simulations. Section 2.1 presents the developed

workflow to translate traffic data into explicit emission sources for the model domain, followed by Section 2.2 introducing the methodological background of the proof-of-concept simulations for this new workflow. Section 2.3 explains the traffic data origin and the processing parameters for emission profile generation, while Section 2.4 introduces the usage of a backwards particle trajectory tracking tool to further analyze air pollution origins.

2.1 Automated Plugin Workflow

To map traffic volumes to a microclimate domain, explicit vehicle trajectory data must be coupled to the road network. This process is fully automated via the newly developed QGIS plugin. The workflow, depicted in Fig. 1, begins by requiring the user to input a vector-based street network, for example derived from OpenStreetMap [45], and a corresponding line-based vehicle trajectory dataset in which each line represents one trip with its start time. Both layers are processed in the projected, metric coordinate reference system of the street layer. Trajectories in another reference system are reprojected automatically. To optimize the spatial representation of the emissions, the plugin discretizes the selected road network into micro-segments based on a user-defined maximum length. This densification step allows the traffic data to be assigned to the ENVI-met domain at the resolution of its micro-scale grid. Following discretization, a localized spatial join is executed: for each micro-segment, all trajectories passing within a user-defined search radius are identified, and each unique trip, identified via a user-specified trip ID field, is counted once per segment. Where parallel street lines lie within the search radius of each other, as for dual carriageways mapped as two separate lines, a trip is counted only on the line it passes closest to, so that the traffic of both directions is not counted on both lines. The counted trips are aggregated into one-hour intervals of a complete 24-hour cycle according to their start

time, matching the hourly resolution of pollutant emission profiles in the ENVI-met database. Because ENVI-met applies emission profiles on its fixed model time zone without daylight saving time, a user-defined time offset shifts the trajectory clock to the model clock, for example by −1 h for trajectories in Central European Summer Time and a model run in UTC+1.

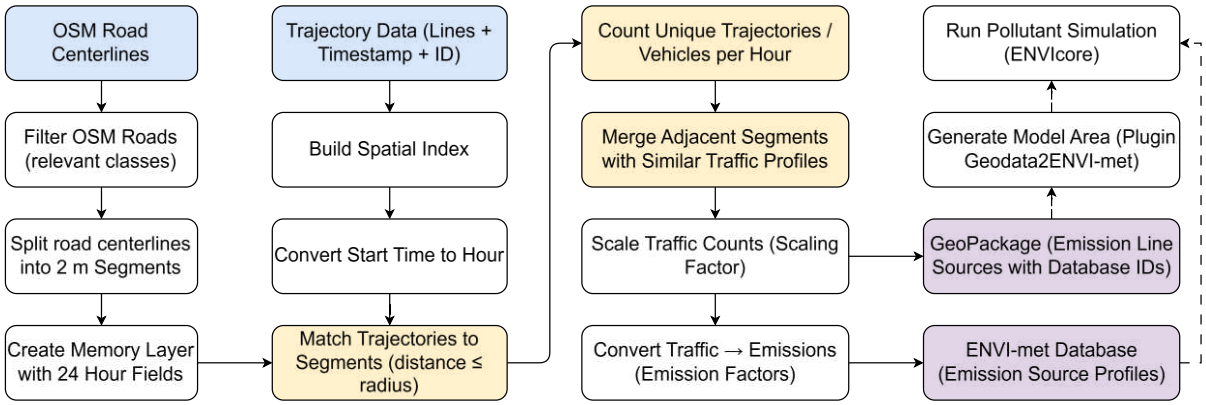


Fig. 1 *Workflow of the Traffic to ENVI-met plugin*

While the fine discretization of the road network preserves the spatial detail of the traffic data, it would introduce significant computational overhead for the model by generating potentially thousands of individual source database items to be imported. To mitigate this without losing relevant spatial detail, the plugin employs an automated topological grouping algorithm. Contiguous road segments are evaluated using a Breadth-First Search algorithm [46]. Touching segments are merged into a single continuous polyline if, in each of the 24-hourly intervals, their vehicle counts differ by no more than a user-defined threshold from those of the group's seed segment. The hourly counts of each merged group are then averaged and rounded to whole vehicles. A GeoPackage file is saved holding the aggregated hourly traffic volumes, total daily traffic volume, and an automatically incremented ENVI-met database ID per street segment.

Following this spatial aggregation, the mathematical recalculations traditionally performed for single road designs within the ENVI-met Traffic Toolbox were

incorporated into the Python workflow to automate the generation of the numerous ENVI-met database items. To obtain the species-specific emission rate per road length $E_{line}\,[ug * m^{-1}s^{-1}]$, the scaled hourly traffic volume $q\,[veh * h^{-1}]$ needs to be converted using the specific emission factor for the target pollutant $EF_{Pollutant}\,[g * km^{-1}]$ and the dimensional conversion constant 3.6 derived from temporal and spatial unit scaling (Eq. 1):

$$E_{line} = \frac{q * EF_{Pollutant}}{3.6} \qquad \textit{Eq. 1}$$

These fluxes are then partitioned into the chemical species required by the model. The NOx emission factor refers to NO_2-equivalent mass, and the user-defined NO_2 fraction is applied on a molar basis, so that the NO mass flux is converted with the molar masses of NO and NO_2 (30.006 and 46.006 g/mol). PM is split by a user-defined PM2.5 fraction of the total PM10 mass, and ENVI-met internally treats the coarse fraction as PM10 minus PM2.5. The hourly fluxes are written to an ENVI-met project database file as 24-hour emission profiles. Because ENVI-met holds each hourly profile value at the full hour and interpolates linearly towards the next one, the value at each full hour is set to the mean of the two adjacent hourly intervals, which centers the emissions in time without changing the daily total. If the output folder already contains a project database, only the emitters written by the plugin are replaced. The emission profile geometries are explicitly defined as line sources (geom: "line") with a height of 0.2 m, following a typical car's exhaust and brake abrasion height.

Utilizing the QGIS plugin Geodata2ENVI-met [47] as a follow-up tool in the automatization workflow, the model area details can then be gridded in the defined horizontal resolution. Only the dominant line-source segment with its specific emission profile database ID is gridded when intersecting with a grid cell. During the simulation,

the ENVI-met core reads the emission source values from the database and scales the mass proportionately across the length of the grid cells that were gridded with the respective emission profile database ID. To test the robustness of the new plugin workflow, proof-of-concept simulations based on the automatized generation of emission profiles were conducted for different days and meteorological conditions.

2.2 Proof-of-concept simulations

The study domain for the proof-of-concept simulations is situated in the Mitte district of central Berlin, Germany, encompassing areas adjacent to Potsdamer Platz and the Brandenburg Gate (Fig. 2). The regional climate is characterized as a temperate, transitional zone (Köppen *Cfb*). Morphologically, the selected domain represents a heterogeneous, densely built-up European city center. The urban fabric is characterized by a high fraction of impervious surfaces and dense building blocks, though it is interspersed with fragmented small parks. The street network exhibits significant geometric variance, ranging from narrow residential streets to major multi-lane roads.

A primary criterion for the spatial delineation of this domain is the inclusion of the official air quality monitoring station at 190 Leipziger Straße (EU-Code: DEBE125), operated by the Berlin Air Quality Network [48]. Situated within an urban street canyon only disturbed by the presence of an arcade-like structure on one street side, this active traffic station continuously records localized concentrations of critical air pollutants, including NO, NO_2, PM10, and PM2.5. The empirical observations from this site effectively capture high-traffic emission profiles and pollution accumulation dynamics, thereby providing a quality-assured reference dataset for the evaluation of the new modeling workflow. According to the Berlin Umweltatlas monitoring, the traffic count for this street exceeds 38,000 vehicles per day [49].



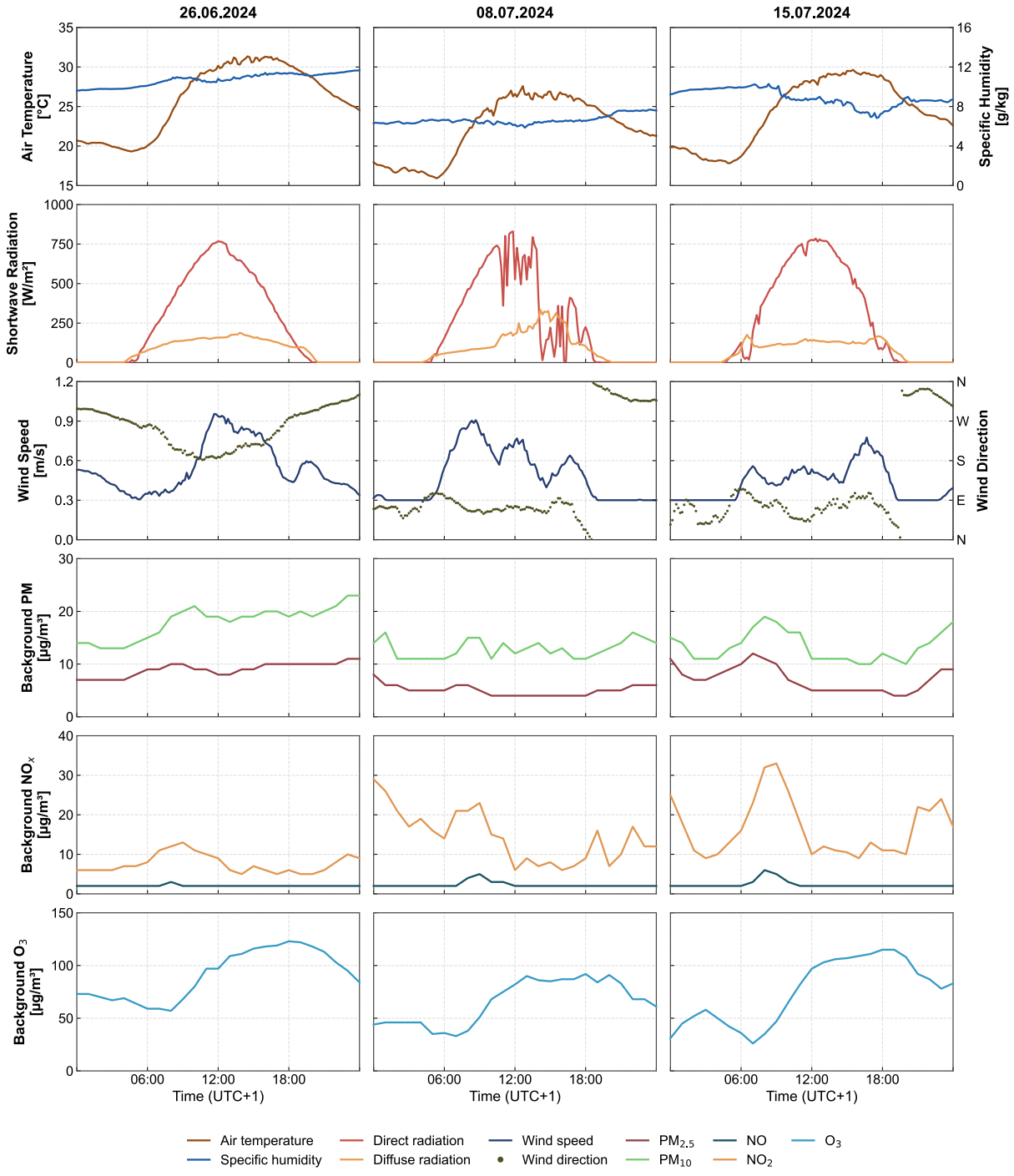
Fig. 2 *Depictions of the study site located at the measurement station 190 Leipziger Straße in Berlin Mitte, Germany, using a detailed map (a) and an overview map within Berlin districts based on OpenStreetMap data (b) [45], and a street view image with an Eastern view direction [photo by author]. Street colors in a) ranging from pink to blue represent traffic volume aggregated for entire day using the new QGIS plugin Traffic Data to ENVI-met. Grey areas indicate impervious surfaces, black areas refer to building footprints in a) and to street surfaces in b). Green areas indicate greened surfaces of parks, green dots display trees. Dimensions of the model domain are depicted by a white dashed line, additionally filled with yellow in b). Blue diamond symbol in a) and yellow rectangle in c) indicate the position of the measurement station*

Simulation settings and model area configuration are summarized in Table 1. The spatial domain was constructed utilizing the QGIS plugin Geodata2ENVImet [47]. To optimize the balance between resolving fine-scale urban morphological features and managing computational demand, the model domain's resolution was set to 2.5 m horizontally and vertically. To accurately capture near-surface thermodynamic processes and the dispersion of vehicular traffic emissions, the lowest vertical grid cell was split into 5 sub-cells of higher resolution.

Table 1 *Simulation settings and model area configuration for the proof-of-concept simulations*

Properties	Values
Start Dates of summer simulations	25.06.2024 / 07.07.2024 / 14.07.2024
Start Dates of autumn simulations	05.11.2024 / 10.11.2024 / 21.11.2024
Start Time (UTC+1)	23:00
Duration [h]	25
Meteorological Boundary Conditions	Full Forcing
Output Interval [min]	60
Location Latitude (Lower Left Corner)	52.507° N
Location Longitude (Lower Left Corner)	13.376° E
Dimensions	315 x 266 x 30
Resolutions (X, Y, Z) [m]	2.5 x 2.5 x 2.5
Lowest Grid Cell Split	Yes
Telescoping: Factor and Starting Height	20 % above 30 m
Height of 3D Model Domain [m]	381.07
Model Rotation out of grid north	-4.78°

Six simulation scenarios were designed to evaluate the urban microclimate under differing atmospheric stability regimes, all starting one hour before midnight to get outputs for all 24 hours of the evaluated day. Additional spin-up time is not needed, as ENVI-met V6 has an internal spin-up implementation now. Furthermore, as the focus of the study is the air pollution module, the thermal initiation of surfaces and objects is less relevant for the simulations of this study. All dates were selected as weekdays outside of public holidays ensuring representative urban anthropogenic emission and traffic profiles to match the average weekday conditions of the trajectory input dataset as good as possible. Dates were selected from the year 2024 to guarantee representative recent traffic volumes, thereby avoiding the anomalous traffic patterns observed during the COVID-19 pandemic (2020-2022) [50].



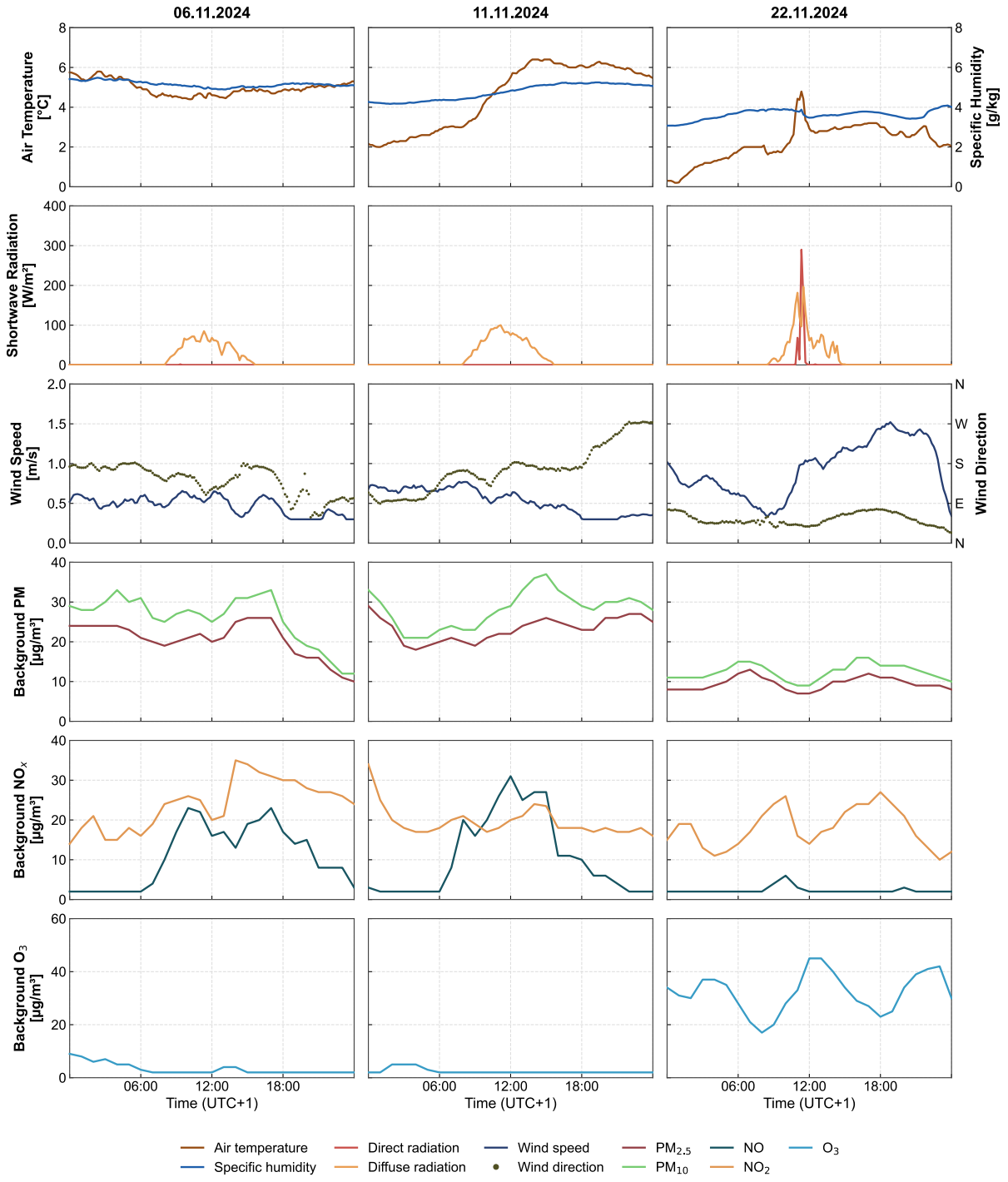
272

273 ***Fig. 3*** *Meteorological boundary conditions including background concentrations for the three summer scenarios*

274 The simulations were executed using the Full Forcing mode in ENVI-met.
275 Meteorological boundary conditions were primarily derived from observational data of
276 the MEVIS measuring network recorded by the Institute of Meteorology of the Freie
277 Universität Berlin after WMO standards [51, 52]. While most data could be obtained

from the MEVIS station 21 Moabit-1 situated in an urban courtyard only 1 km North of the model domain [53], solar radiation could only be derived as global shortwave radiation. We hence obtained it from German Weather Service (DWD) measurement station Berlin-Brandenburg (Station ID: 00427), where solar radiation data were extractable as direct and diffuse components. Longwave radiation was set to 0 in the Forcing File to let the ENVI-met simulation handle the calculation of the parameter based on atmospheric temperature, humidity, and cloud conditions.

The first three scenarios (Wednesday, 26.06.2024 / Monday, 08.07.2024 / Monday, 15.07.2024) represent convective summer conditions, characterized by diurnal air temperatures ranging from 15 °C to 32 °C with low wind speeds and mostly clear sky conditions (Fig. 3). The second three scenarios (Wednesday, 06.11.2024 / Monday, 11.11.2024 / Friday, 22.11.2024) reflect rather stable, overcast autumn/winter conditions with low air temperatures between 0 and 6 °C (Fig. 4). While mostly representing calm wind situations only up to 1 m/s as well, 22nd of November featured comparatively high wind speeds of 1.5 m/s. Very low wind speeds can cause instabilities and crashes for CFD models and should hence be avoided as input. As the wind speed values were measured in the comparatively low height of 3 m, we were able to clamp the values at only 0.3 m/s and could still conduct stable model runs. Maintaining real wind speed patterns as accurately as possible was fundamental since that is the major driver for the distribution of particles investigated in this study. While air temperature, relative humidity, and radiative fluxes are often equally or even more important in ENVI-met's typical use cases related to thermal comfort studies [54–56], they also matter for air quality: shortwave radiation drives the photolysis of NO_2 in the $NO–NO_2–O_3$ cycle, and surface heating and the resulting stability control the vertical mixing in the street canyon.



303

304 ***Fig. 4*** *Meteorological boundary conditions including background concentrations for the three autumn/winter*
305 *scenarios*

306 To accurately capture the surrounding urban background pollution, background
307 pollutant concentrations for the model were obtained by taking the median of the
308 background monitoring stations 010 Wedding, 042 Neukölln, and 171 Mitte (EU-

Codes: DEBE010, DEBE034, DEBE068) [57–59]. Besides PM10 and PM2.5, the forced background comprises NO, NO_2 and O_3, which the NO–NO_2–O_3 chemistry requires. While standard meteorological parameters (air temperature, humidity, shortwave radiation, and wind) can be imported directly into ENVIguide's FOX file creation via a CSV file, the current graphical user interface of ENVI-met lacks native support for importing background concentration time series into the forcing file (.FOX). Therefore, a custom Python script was used to generate the FOX file based on the different input parameters. Consequently, the simulation configuration file (.SIMX) was manually modified by adding the forceBackgrConc parameter to the Full Forcing section with the value of 1, thereby activating the background concentration forcing for the simulation. The forced background concentrations are prescribed at the inflow boundaries of the model domain and updated every 10 minutes.

The simulations were performed with ENVI-met V6. Its gas-phase chemistry module transports NO, NO_2 and O_3 as separate species and, after each transport step, integrates the reactions $NO + O_3 \rightarrow NO_2 + O_2$ and $NO_2 + h\nu \rightarrow NO + O_3$ with an exact closed-form solution, which conserves NOx and Ox ($NO_2 + O_3$) in every grid cell. The model therefore does not assume a photostationary state but relaxes towards it at a rate set by the local concentrations and the photolysis frequency. The photolysis frequency $J(NO_2)$ is derived from the global radiation on an unobstructed horizontal surface using the empirical relation of Trebs et al. [60] and is distributed to each grid cell according to its direct-beam transmission and its sky view, weighted by the diffuse share of the actinic flux in the UV-A range. For a street canyon with an aspect ratio of about one, this yields a mean $J(NO_2)$ of about 40 % of the open-air value at street level around noon, in line with radiative transfer studies of street canyons [61]. The chemistry of volatile organic compounds (VOCs) and peroxy radicals is not represented.

2.3 Emission Profile Generation

Traffic volumes were quantified using a dataset of individual vehicle trajectories, which have been generated with SUMO (Simulation of Urban Mobility), an open-source tool used to simulate continuous intermodal traffic [62]. For the purposes of this experiment, we selected a SUMO scenario for Berlin that aims to represent the car traffic volume of an exemplary/average day [63, 64]. Each trajectory represented a complete, continuous car trip possessing a start time in seconds after midnight. While the scenario theoretically aims to represent 100 % of an average day's car traffic volume, evaluations of this dataset against empirical traffic counts have demonstrated a systematic tendency to underestimate vehicle numbers on larger multi-lane roads [64]. According to official Berlin traffic data, the target segment of Leipziger Straße experienced an average weekday volume of approximately 38,000 motorized vehicles in 2019, a level considered representative for current baseline conditions [49] (Section 2.2). The SUMO dataset contains only around 2,500 vehicles per day for this street segment. To correct for this underrepresentation, a uniform scaling factor of 15 was applied to the averaged counts of each geometry prior to the flux calculation, which brings the simulated volume at the street segment next to the measurement station close to the 38,000-vehicle target. This approach carries inherent limitations. Neighboring streets are less underrepresented in the SUMO scenario and would have required factors of only 5 to 7, so that the uniform factor overestimates their traffic and elevates emissions and concentrations across the wider model domain. Additionally, the empirical count of 38,000 from Berlin’s Umweltatlas encompasses all motorized vehicles, including high-emitting classes such as heavy-duty trucks, municipal buses, and motorcycles, which are absent from the passenger-car-only trajectory dataset. Lastly, the underlying SUMO trajectories represent an average day under fluent traffic

conditions, largely omitting the emission-intensive stop-and-go dynamics induced by local traffic lights and congestion, and their diurnal profile at the station segment peaks in the afternoon rather than in the morning rush hour.

For the generation of emission profiles for the proof-of-concept simulations, the road network base dataset was sourced from OpenStreetMap and filtered to isolate primary, secondary, residential, and associated link roads [45]. During the plugin processing, the maximum length for the micro-segment discretization was set to 2 m, slightly smaller than the 2.5 m horizontal grid resolution of the ENVI-met domain, so that curved road geometries were captured accurately during the subsequent gridding process. The spatial join search radius was set to 5 m to capture trajectories across the standard width of urban road lanes, including lane changes and junction traffic, without falsely incorporating trajectories from adjacent, parallel streets. To manage the database size, the threshold for the topological grouping was set to 3 vehicles per hour, which significantly reduced the number of individual ENVI-met database IDs while preserving the localized traffic volume gradients. Since the SUMO trajectories follow local clock time, the time offset was set to −1 h for the summer scenarios (Central European Summer Time) and to 0 h for the autumn scenarios. This results in two emission databases with identical source geometries and database IDs that differ only in the timing of their hourly profiles, so that the same gridded model area serves both seasons.

Pollutant emission rates were derived using modern passenger car emission factors adapted from the European Environment Agency's EMEP/EEA air pollutant emission inventory guidebook [5]. Reflecting a modern urban fleet characterized by efficient exhaust filtration but significant non-exhaust emissions, the base factors were set to 0.180 g/km for NOx and 0.020 g/km for total PM. The PM factor explicitly accounts for

non-exhaust abrasion from brake wear, tyre wear, and road surfaces, which now widely exceed exhaust emissions in European urban fleets [5]. To partition these base factors into the species required by the atmospheric chemistry model, the NO_2 fraction of NOx was set to 0.2 and the PM2.5 fraction of PM10 to 0.6 following generalized estimations of modern car fleet emissions based on the EMEP/EEA guidebook [5]. Consequently, 20 % of the NOx (on a molar basis) was emitted as primary NO_2 and 80 % as NO, while PM2.5 was assumed to constitute 60 % of the total PM10 mass.

2.4 Backwards Particle Trajectory Tracking

To accurately determine the spatial origin of the modeled pollutants reaching the Leipziger Straße measurement station, an advanced footprint analysis was conducted. It serves to verify that the localized pollutant accumulation observed in the diurnal cycles represents micro-scale wind field dynamics rather than an artifact of erroneous Eulerian pollutant transport. Specifically, the analysis aimed to confirm whether the modeled concentration peaks were affected by immediate local traffic emissions, or if they were influenced by intra-urban transport from other heavily trafficked roads within the broader simulation domain.

For this purpose, the Lagrangian Stochastic Trajectory Model (LaStTraM) was utilized [65, 66]. LaStTraM is a post-processing tool specifically designed to couple with the holistic, three-dimensional microclimate outputs of ENVI-met, hence representing the first building-resolved Lagrangian stochastic footprint prediction model. To maximize computational efficiency, LaStTraM employs a backward-integration approach. Instead of simulating the forward dispersion of particles from every emission source across the entire model domain, where most particles would never reach the sensor, the model releases particles directly from the detector and tracks their trajectories backward in time until they reach an emission source. The advection of these particles is computed

using the Lagrangian Stochastic method, which calculates the particles' velocity using both a resolved, deterministic component derived from ENVI-met's interpolated 3D wind vectors, and a stochastic component representing subgrid-scale turbulent kinetic energy. While LaStTraM was originally validated using vegetation-based vapor fluxes, we adapted the codebase to link the backward-tracked footprints to the traffic emission sources. For the footprint simulations, the detector size was defined to be 2 x 2 x 2 meters at x: 405 m, y: 312 m, z: 2 m to match the exact grid coordinates of the Leipziger Straße measurement station. To ensure a statistically robust probability distribution of the concentration footprint, an ensemble of 20,000,000 particles was released from the detector for every hourly output available.

3 Results

This section presents the evaluation of both the proof-of-concept simulations generated via the QGIS plugin Traffic Data to ENVI-met and the backwards particle trajectory modeling. The modeled concentrations of PM2.5 and PM10 as well as NO and NO_2 at the grid cell of the Leipziger Straße monitoring station (1.75 m above ground) were compared against its hourly observations on six days in 2024, representing summer and autumn conditions. Model performance is expressed by the squared Pearson correlation coefficient (R^2), the root mean square error (RMSE) and the mean bias (MB, modeled minus measured), complemented by the fraction of values within a factor of two of the observations (FAC2), the fractional bias (FB) and the normalized mean square error (NMSE), for which acceptance criteria for urban dispersion models exist [67]. At first, the overall model performance at the measurement site is analyzed using linear regression (Section 3.1), followed by diurnal cycle analyses per day and pollutant type (Section 3.2). Section 3.3 separates the local

concentration increment from the forced background. Lastly, the spatial distribution of pollutants and the particle origin are investigated (Section 3.4).

3.1 Overall Model Performance

The global regression analysis for the measurement site grid cell across all simulated days reveals clear differences between the particulate and the gaseous pollutants (Fig. 5). PM2.5 showed the highest agreement, with a global R^2 of 0.94, an RMSE of 2.1 µg/m³ and a mean bias of only +0.5 µg/m³. PM10 also agreed well, with an R^2 of 0.82, an RMSE of 3.7 µg/m³ and a mean bias of −0.7 µg/m³. The modeled PM values cluster along the 1:1 line, and all data points of both fractions fall within the factor-of-two (FAC2) bounds. Because the six days span very different regional pollution levels, from about 5 µg/m³ PM2.5 in July to about 30 µg/m³ in November, these global statistics largely reflect how well the dynamic background forcing reproduces the day-to-day variation (Section 3.2).

The reactive gases showed more complex patterns. NO was captured in its temporal variation with a global R^2 of 0.80, but with an RMSE of 14.1 µg/m³ and a systematic underprediction (MB = −7.8 µg/m³). The regression slope remains well below unity: concentration spikes are registered, but their magnitude is underestimated, with modeled values between about 30 and 70 µg/m³ where the measured peaks reached 70 to 120 µg/m³, partly outside the FAC2 bounds. NO_2, in contrast, showed almost no overall bias (MB = +0.8 µg/m³) and an RMSE of 9.3 µg/m³, but the lowest correlation (R^2 = 0.34). Most NO_2 data points lie within the FAC2 bounds, yet they scatter widely around the 1:1 line, indicating that the NO_2 level is matched while its temporal course is not. Against the acceptance criteria for urban dispersion models (FAC2 ≥ 0.3, |FB| ≤ 0.67, NMSE ≤ 6), all four pollutants met all three criteria in the global evaluation (Table

2). On individual days, only NO on July 15 slightly exceeded the FB criterion (FB = 0.69), reflecting its underprediction.

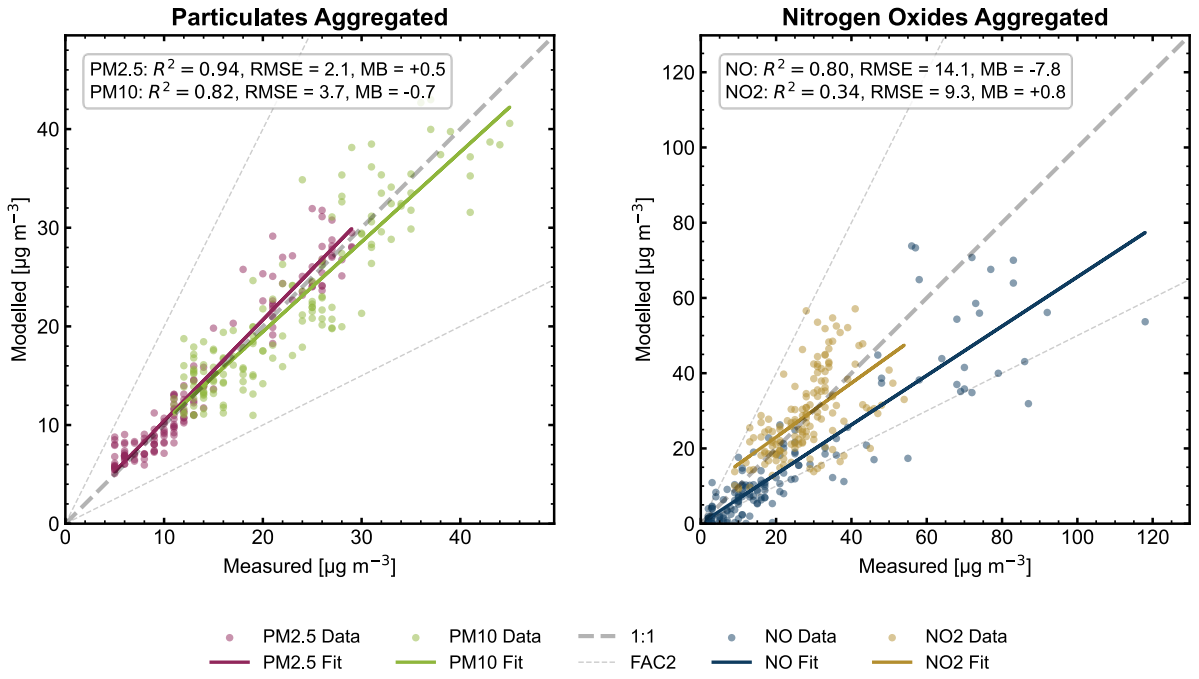


Fig. 5 *Linear regression of modeled against measured hourly concentrations of PM (left) and NO and NO_2 (right) at the station grid cell for all six days, with R^2, RMSE and mean bias (MB) in µg/m³. Dashed lines mark the 1:1 line and the factor-of-two bounds*

Table 2 *Global performance measures at the station grid cell for all six days and the acceptance criteria for urban dispersion models [67]. FB is positive for underprediction*

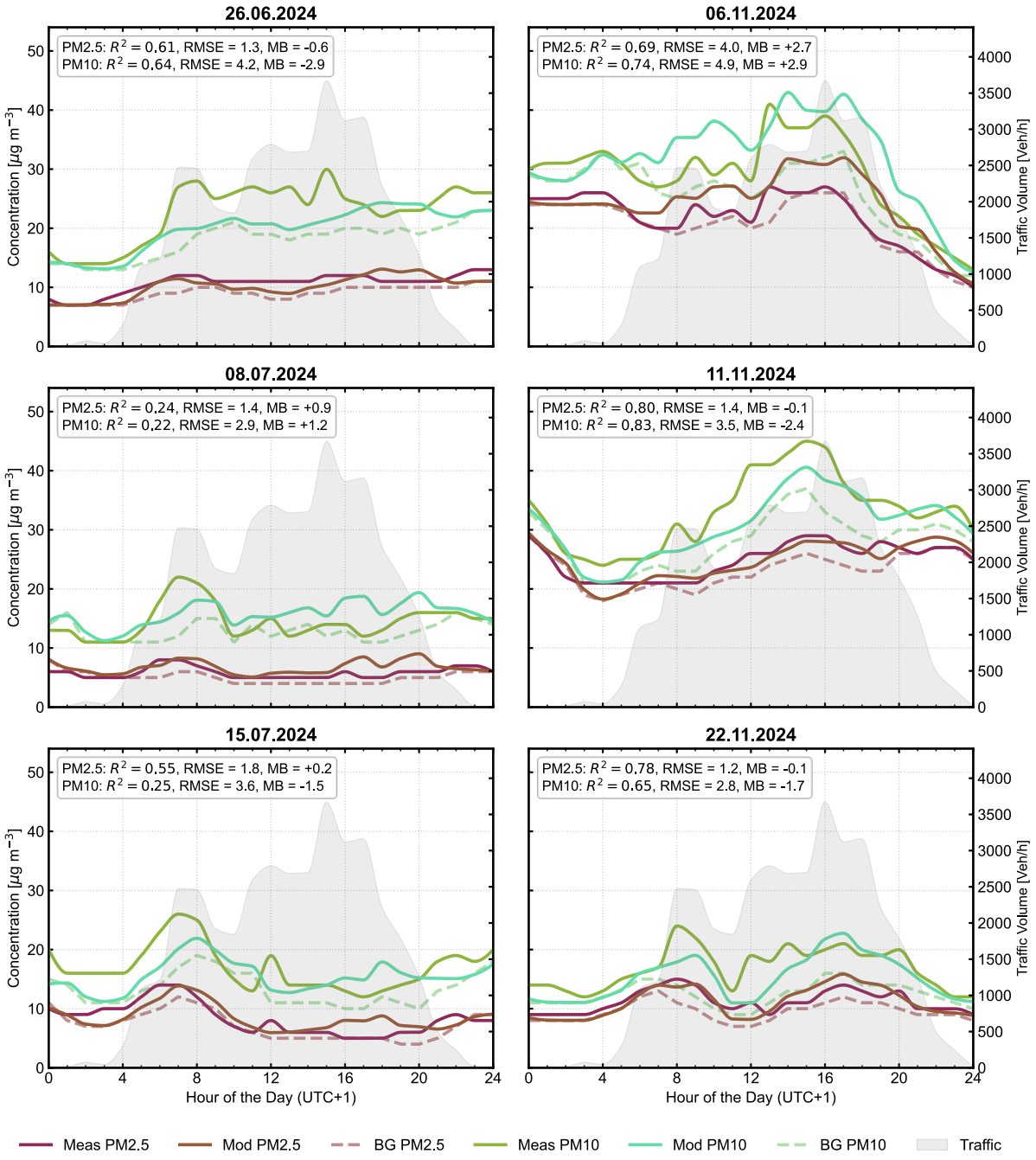
Pollutant	FAC2	FB	NMSE
PM2.5	1.00	−0.04	0.02
PM10	1.00	0.03	0.03
NO	0.62	0.41	0.57
NO_2	0.95	−0.03	0.11
Criterion	≥ 0.30	−0.67 to 0.67	≤ 6

3.2 Diurnal Concentration Dynamics

The diurnal cycles provide insight into the temporal performance of the model across the day (Fig. 6, Fig. 7). For the gaseous pollutants, the modeled concentrations clearly

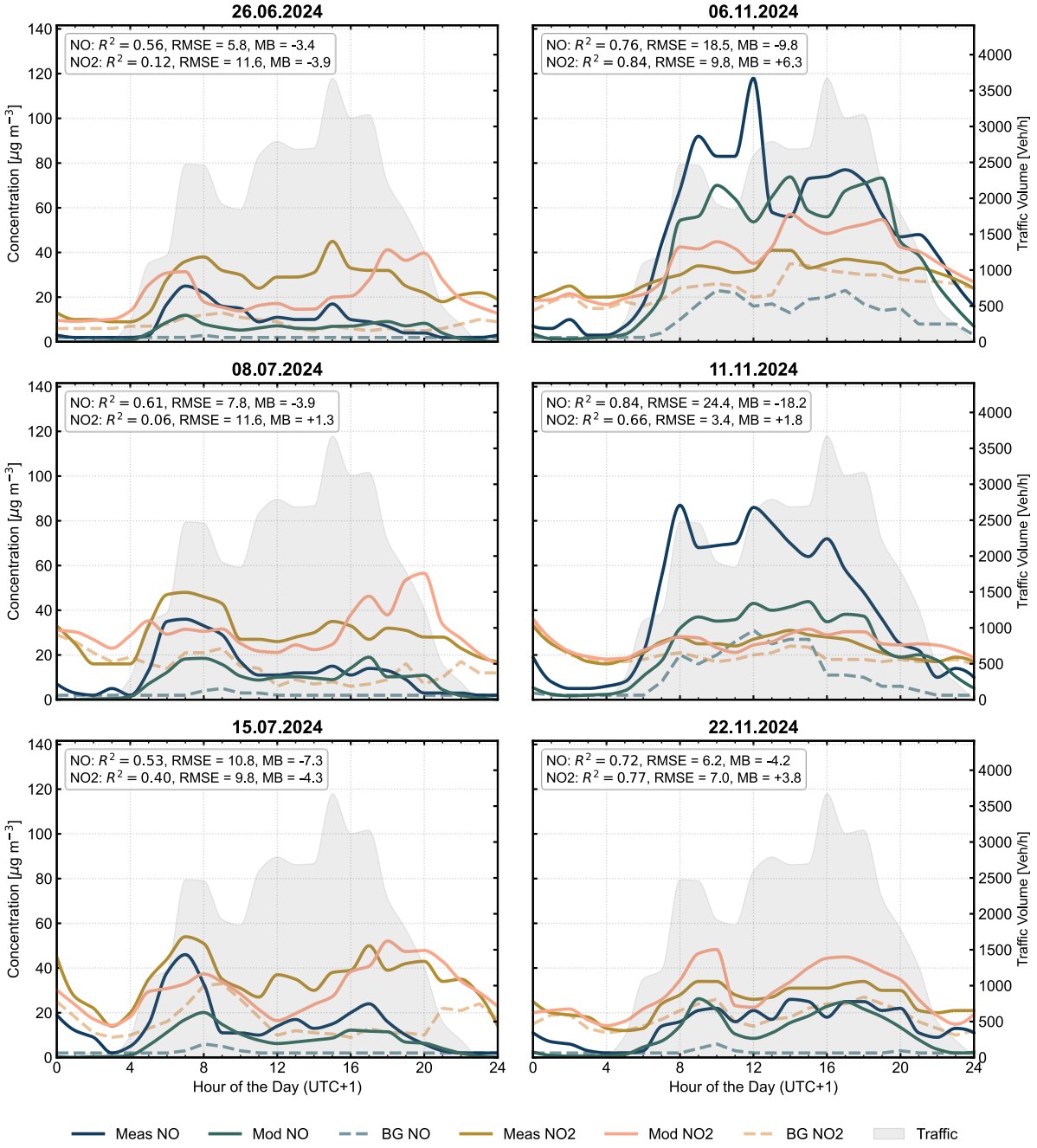
separate from the forced background during periods of elevated traffic volume, reflecting the local emission signal superimposed on the regional baseline within the street canyon. For PM, this local increment is small, and the modeled PM2.5 and PM10 concentrations stay close to their forced background concentrations on most days (Section 3.3).

On individual days, the agreement for PM varies with the season. The autumn days show the highest per-day correlations (R^2 of 0.69 to 0.80 for PM2.5 and 0.65 to 0.83 for PM10), as the modeled concentrations follow the pronounced background variations, for example the afternoon maximum on November 11 and the evening decline on November 6. On the summer days, the regional PM level is low and varies little, so that the per-day correlations are weaker (R^2 of 0.24 to 0.61 for PM2.5 and 0.22 to 0.64 for PM10) despite small errors (RMSE ≤ 1.8 µg/m³ for PM2.5). During the summer daytime, the measured PM10 frequently exceeded the modeled values, most notably on June 26 with measured values of 25 to 30 µg/m³ against about 20 µg/m³ modeled (MB = −2.9 µg/m³), while PM2.5 was matched closely. The largest positive bias occurred on November 6 (MB = +2.7 µg/m³ for PM2.5 and +2.9 µg/m³ for PM10), when the modeled PM10 rose to about 43 µg/m³ in the afternoon compared with 37 µg/m³ measured at the same hour. Overall, the temporal evolution of the modeled PM follows the advected background and is modulated by the local meteorological conditions rather than by the traffic profile, which emphasizes the need to include background concentration forcing in such studies.



491

492 ***Fig. 6*** *Diurnal cycle of measured (dark colors) and modelled (light colors) PM values (PM2.5 and PM10), their*
493 *respective forced background concentrations (dashed lines), and traffic volume at the street segment near*
494 *measurement station 190 Leipziger Straße for all six simulated days. Statistics refer to the hourly values of each*
495 *day; the time axis shows the model time (UTC+1)*



496

497 ***Fig. 7*** *Diurnal cycle of measured (dark colors) and modelled (light colors) nitrogen oxide values (NO and NO_2), their*
498 *respective forced background concentrations (dashed lines), and traffic volume at the street segment near*
499 *measurement station 190 Leipziger Straße for all six simulated days. Statistics refer to the hourly values of each*
500 *day; the time axis shows the model time (UTC+1)*

501 The diurnal cycles of the reactive gases reveal a consistent underprediction of NO (Fig.
502 7). On all six days, the modeled NO remained below the measurements (MB of −3.4
503 to −18.2 µg/m³), while its timing was captured well (R^2 of 0.53 to 0.84). In summer, the

504 measured NO peaked during the morning rush hour at 25 to 46 µg/m³, whereas the
505 modeled morning maxima reached only 12 to 20 µg/m³, about half of the measured
506 values, at the same hour or up to one hour later. On the stable autumn days, NO
507 accumulated strongly in the street canyon, and the measurements peaked at 87 to 118
508 µg/m³ on November 6 and 11. The model reproduced the shape of these episodes but
509 with lower magnitudes, reaching about 70 to 74 µg/m³ on November 6 and only about
510 44 µg/m³ on November 11 (MB = −18.2 µg/m³). On November 22, with comparatively
511 high wind speeds, modeled and measured NO were both moderate and agreed closely.
512 For NO_2, the model reproduced the overall level but not the diurnal course in summer
513 (R^2 of 0.06 to 0.40). The measured NO_2 peaked in the morning at 38 to 54 µg/m³, while
514 the modeled NO_2 remained lower in the morning but rose to its maxima of 41 to 57
515 µg/m³ in the late afternoon and evening, when the measured values had already
516 decreased, most clearly on July 8. In autumn, the diurnal course of NO_2 was captured
517 better (R^2 of 0.66 to 0.84), but the model overpredicted NO_2 by 1.8 to 6.3 µg/m³ on
518 average, with modeled afternoon values of 50 to 57 µg/m³ on November 6 against
519 measured values of 33 to 41 µg/m³. Hence, in autumn the model assigns a larger share
520 of the NOx to NO_2 than observed, while its NO is too low (Section 3.3). In general, the
521 measured NO and NO_2 showed a stronger morning than afternoon peak, whereas the
522 modeled concentrations rather follow the traffic input profile, which peaks in the
523 afternoon.

524 **3.3 Local Concentration Increment**

525 Because modeled concentrations inherently contain the forced background
526 concentrations, the agreement of the total concentrations does not show how well the
527 local traffic contribution is reproduced. The local increment was therefore evaluated
528 separately as the hourly concentration minus the forced background, for both the

529 measured and the modeled values (Fig. 8). NOx was evaluated as the sum of NO and
530 NO_2 in NO_2-equivalent mass, which the gas-phase reactions conserve, so that its
531 increment reflects the local emissions and their dilution independently of the chemical
532 partitioning.

533 For PM, the local increment is small. The measured PM2.5 and PM10 concentrations
534 exceeded the background by 1.3 and 3.8 µg/m³ on average, or 10 % and 17 % of the
535 measured concentrations. The modeled increments were of similar size (1.8 and 3.0
536 µg/m³), but their hourly variation was unrelated to the measured one (R^2 = 0.02 for
537 PM2.5 and 0.08 for PM10; Fig. 8a), partly because the measured increments are close
538 to the 1 µg/m³ resolution of the reported observations.

539 For NOx, the local increment dominated the measured concentrations, with a mean of
540 38.3 µg/m³ above a background of 24.5 µg/m³. The model reproduced 71 % of it (27.2
541 µg/m³), and the hourly increments correlated with an R^2 of 0.48 (Fig. 8b). On individual
542 days, the modeled share ranged from 47 % on November 11 to 90 % on November
543 22, with 57 to 84 % on the summer days (Fig. 8c). Of the NO increment alone, the
544 model reproduced only 56 %, as a larger part of its NOx increment consisted of NO_2.
545 The split of the NOx increment into NO and NO_2 differed consistently between model
546 and measurements (Fig. 8c). On all six days, the model assigned a larger share of the
547 increment to NO_2 than observed, by 11 to 19 percentage points. On the summer days,
548 with background ozone concentrations of 65 to 91 µg/m³ on average, NO_2 accounted
549 for 50 to 63 % of the measured and 64 to 74 % of the modeled increment. On
550 November 6 and 11, the background ozone was nearly exhausted (3.3 and 2.4 µg/m³
551 on average), so that little of the emitted NO could be converted to NO_2. On these days,
552 NO_2 accounted for only 8 to 9 % of the measured increment but for 23 to 24 % of the

modeled one, close to the primary NO_2 fraction of 20 % assumed for the passenger-car fleet in the emission input (Section 2.3).

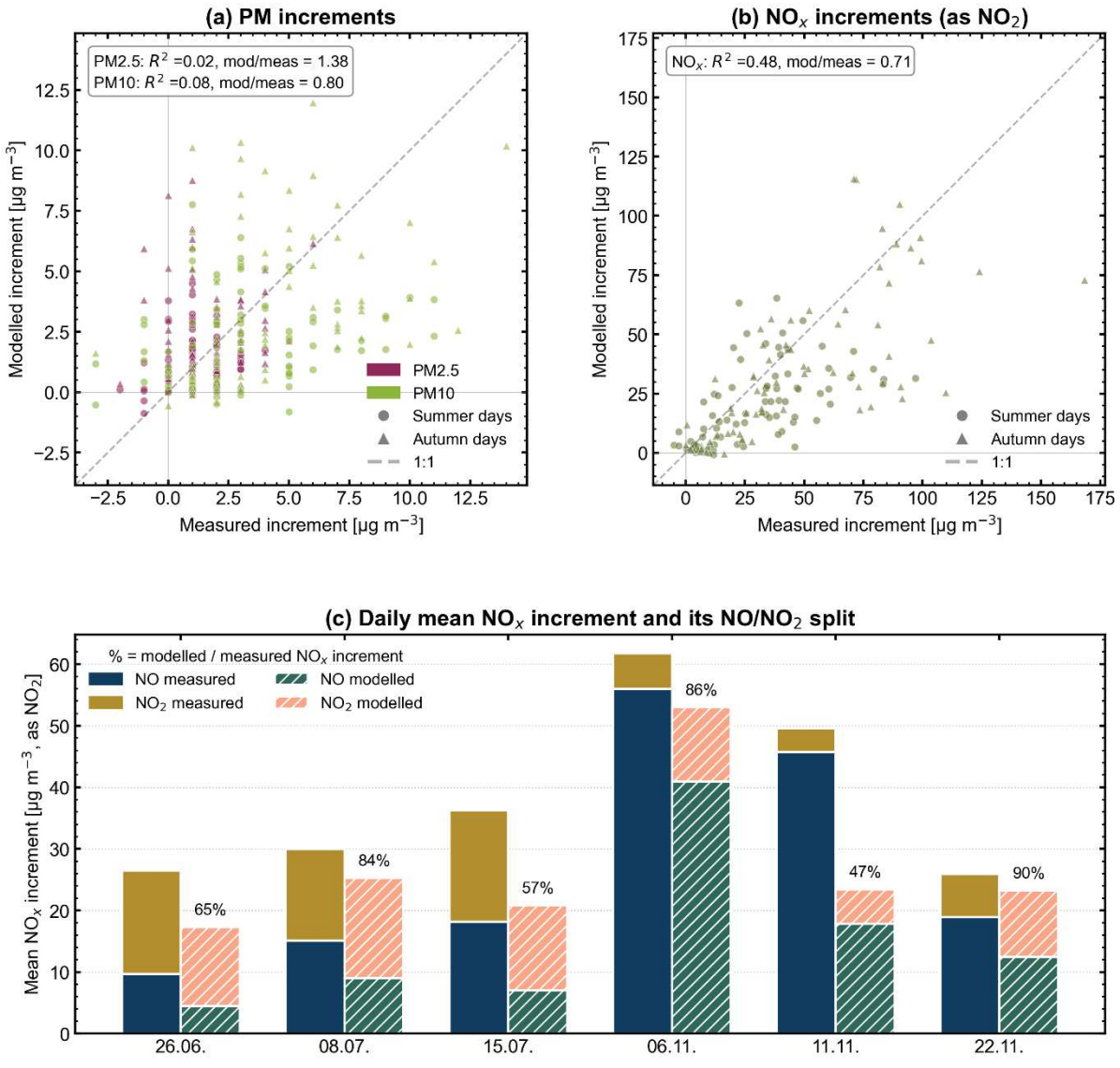


Fig. 8 *Local concentration increment at the station grid cell, defined as the hourly concentration minus the forced background, measured against modelled for all six days: (a) PM2.5 and PM10 and (b) NOx as NO_2-equivalent, with R^2 and the ratio of the mean modelled to the mean measured increment; (c) daily mean NOx increment split into NO (as NO_2-equivalent) and NO_2, with the modelled increment in percent of the measured one. Measured PM increments take discrete values, as the PM observations are reported in whole µg/m³*

3.4 Spatial Analysis

Beyond temporal dynamics, the exemplary spatial distribution map of NO during the morning rush hour at 08:00 on November 6, when the modeled NO at the station was

within about 20 % of the measured value, reveals distinct differences between the urban canyons that are strongly dependent on the emission sources and localized wind patterns (Fig. 9). As established in the diurnal analysis, the aerodynamic confinement of the dense urban geometry under low wind speeds leads to a pronounced accumulation of vehicular emissions. The spatial map visualizes this heterogeneity, demonstrating that the pollutant buildup is sensitive to the immediate urban environment. While the Leipziger Straße measurement site exhibits localized pollution accumulation, other urban street canyons within the modeled domain reach or even exceed these concentration values depending on their geometric orientation to the prevailing wind and their traffic volumes. On the neighboring multi-lane roads, part of these high values results from the uniform scaling factor, which overestimates their traffic (Section 2.3).

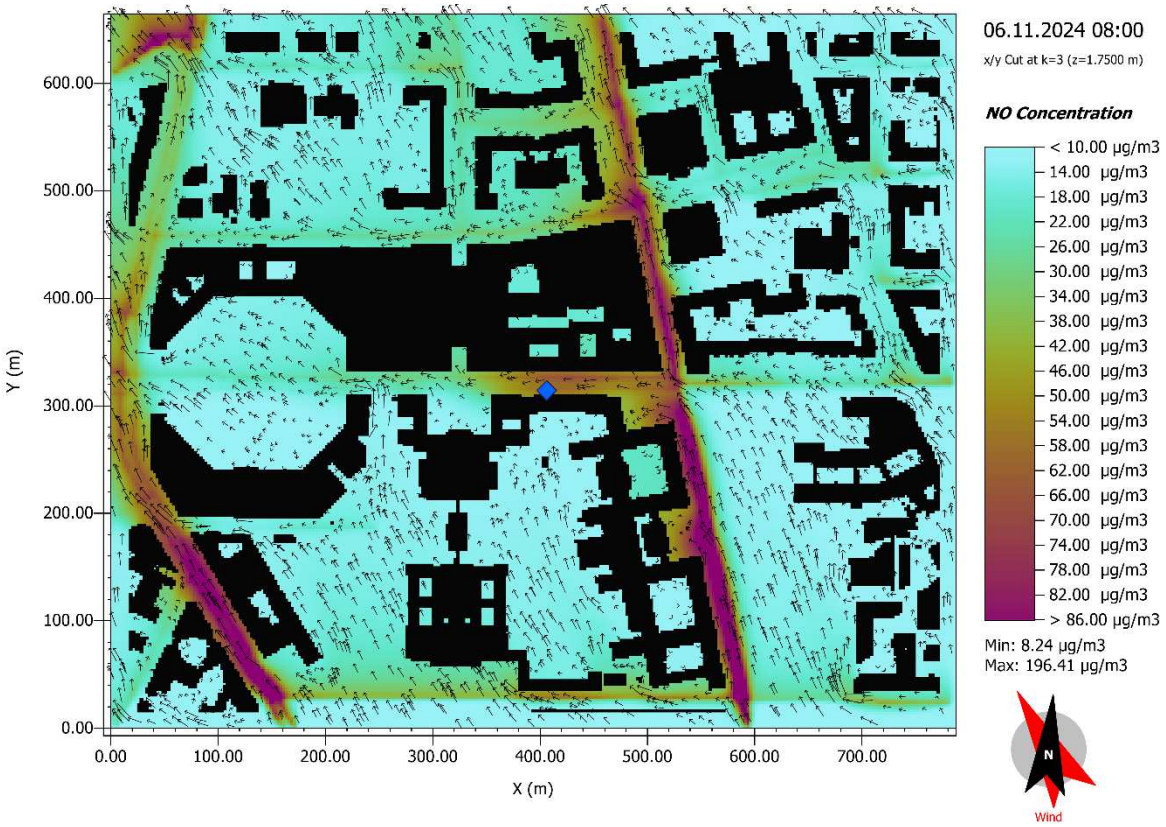


Fig. 9 *Spatial distribution map of NO with wind vectors for the height level of 1.75 m above ground on 6th of November, 2024, 08:00. Blue diamond symbol indicates the position of the measurement station*

To further investigate the spatial origins of the pollutants reaching the measurement station, the footprints computed with the LaStTraM post-processing tool were evaluated. The spatial distribution map of accumulated particle origins for one exemplary day (15th of July) visualizes the source areas contributing to the modeled air pollution within the detector volume of the measurement station (Fig. 10). The backward trajectory analysis reveals that the vast majority of particles arriving at the measurement station originate almost exclusively from its immediate surrounding street canyon. Aside from the direct vicinity, only one additional, notable origin hotspot is identifiable at a nearby high-traffic junction. The other simulation scenarios were also post-processed and showed similar results with a slightly more or less pronounced secondary hotspot at the nearby traffic junction.

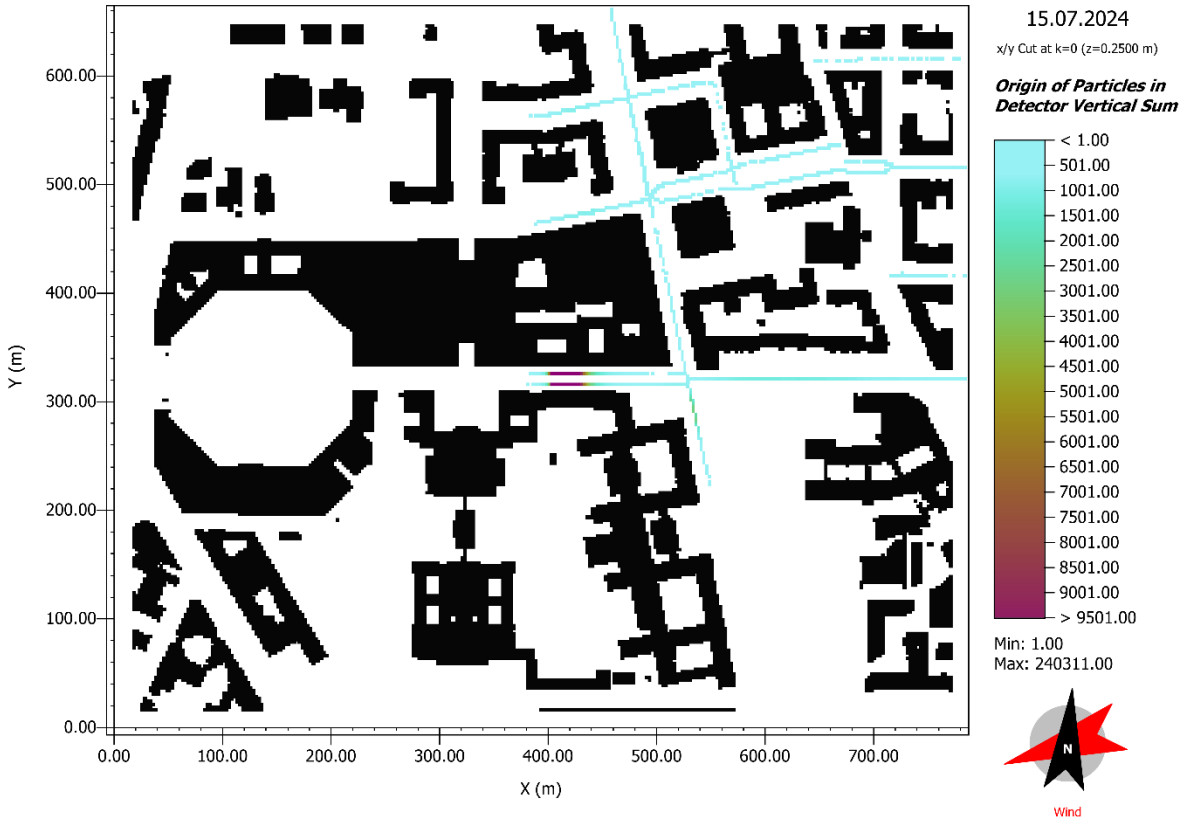


Fig. 10 *Spatial distribution map of total accumulated particle origin counts in detector after backwards trajectory modelling using LaStTraM for the entire simulation period at 15th of July, 2024*

4 Discussion

While the QGIS workflow addresses the spatial data-entry bottleneck associated with micro-scale dispersion modeling, both the agreement and the deviations found in the proof-of-concept evaluation need to be put into the context of the model physics and the input data. The following sections discuss what the agreement for PM rests on and how the diurnal timing arises (Section 4.1), what controls the NO/NO_2 partitioning in the model (Section 4.2), which input assumptions limit the simulation of traffic-related NOx (Section 4.3), and how robust the evaluation is (Section 4.4).

4.1 PM Dispersion Dynamics and Spatial Footprints

The footprint analysis offers a check on the Eulerian pollutant transport, as LaStTraM uses the wind and turbulence fields of ENVI-met but calculates the subgrid-scale particle dispersion with its own stochastic scheme based on Gaussian randomization [68–72]. With a source area confined to the adjacent street canyon and a nearby junction, and practically no transport from more distant roads (Section 3.4), the concentration increment above the forced background at the station is a local signal, set by the emissions of the adjacent street segments and the ventilation of the canyon. As the PM increment is small and its hourly variation is not reproduced (Section 3.3), the high global agreement for PM (Section 3.1) reflects the background forcing, which is derived from three urban background stations of the same monitoring network. The evaluation of the local traffic contribution therefore rests on the NOx increment.

The diurnal timing of the modeled concentrations closely follows the traffic input, whose trip start times were converted to the model time zone (Section 2.3). As the SUMO profile at the station segment peaks in the afternoon, the modeled concentrations lack the pronounced morning maximum of the measured NO and NO_2. Two factors

contribute to this maximum: a morning traffic peak that is more pronounced in reality than in the average-day scenario for this street segment, including delivery and heavy-duty traffic, and the shallow, stable morning boundary layer, which accumulates emissions before the onset of convective mixing. On the summer days, the modeled NO_2 maxima in the late afternoon and evening coincide with high traffic volumes, decreasing photolysis and weakening vertical mixing, which together favor the accumulation of NO_2 in the canyon at a time when the measured values had already declined.

Remaining discrepancies in the PM simulations, particularly the underprediction of PM10 during summer daytime and on days with higher wind speeds, likely stem from coarse particle sources that the model does not include, such as wind- and traffic-induced resuspension of road dust. In addition, the PM emission factor of 0.020 g/km for a passenger-car fleet in fluent traffic excludes the brake and tire wear of heavy-duty vehicles and buses as well as the additional abrasion in stop-and-go traffic. The fixed assumption that PM2.5 constitutes 60 % of the PM10 emissions further prevents the model from adapting to variations in PM composition. The overprediction on November 6 coincides with the most stagnant conditions of the six days and indicates that the local PM increment is sensitive to the simulated ventilation of the canyon at very low wind speeds.

However, the small PM increment does not make traffic emissions irrelevant for PM simulations. Increments of a few µg/m³ at roadside sites are typical for modern vehicle fleets with largely reduced exhaust particle emissions [73–75], and the measured mean increments of 1.3 µg/m³ for PM2.5 and 3.8 µg/m³ for PM10, although derived from six days only, correspond to about 13 % and 19 % of the annual limit values applicable from 2030 (Section 1). Moreover, microscale simulations rarely aim at the

total concentration at a single site, which a background station already provides. Their value lies in the spatial distribution within the street space, for example between sidewalks, courtyards and the windward and leeward sides of a canyon, and in the comparison of planning scenarios such as tree planting or traffic measures, in which the background cancels out and only the local increment differs. These applications depend on segment-specific emission input of the kind the plugin provides.

4.2 NO/NO_2 Partitioning and Model Chemistry

Unlike PM, the partitioning between NO and NO_2 is governed by fast chemical reactions. Close to the sources, freshly emitted NO is converted to NO_2 mainly by reaction with ozone, while the photolysis of NO_2 reforms NO and O_3 during daytime. Since the model integrates both reactions in time in every grid cell (Section 2.2), the modeled NO_2/NOx ratios near the emission sources remain below their photostationary values. The VOC chemistry omitted by the model is of minor importance here: on the time scale of minutes on which air is exchanged between the canyon and the air above, peroxy radicals contribute little to the conversion of NO into NO_2 compared with the reaction with ozone [76], and their effect on the regional NO_2 and O_3 levels is contained in the forced background concentrations. While the software has an oxidation scheme implementation for biogenic isoprene [33], this scheme is not yet publicly available and was disabled in this study.

Consequently, the chemistry scheme alone does not explain the deviations in summer. On the summer days, NO was underpredicted by about half during the morning rush hour, while the modeled NO_2 level was close to the measured one. With high ozone background concentrations in summer, a large share of the emitted NO is converted to NO_2 within the canyon, so that the modeled NO_2 is relatively insensitive to the emitted amount of NOx, whereas NO responds directly to it. The underprediction of

NO therefore combines two effects that the increment analysis separates (Section 3.3): a smaller NOx increment than measured, which indicates too low local NOx emissions or too strong dilution in the model (Section 4.3), and a larger NO_2 share of this increment. The misplaced diurnal maxima of NO_2 follow the traffic input and the evening meteorology (Section 4.1). While enabling VOC chemistry could raise the modeled NO_2 during the day, it could not remove its excess in the evening.

In autumn, the ozone background concentrations were low, and the conversion of NO to NO_2 within the canyon was limited by the available ozone. Under these conditions, the measured NO accumulated to 80 to 120 µg/m³ on November 6 and 11, while the measured NO_2 remained moderate, as its formation was bounded by the ozone supply and the primary NO_2 emissions. The model reproduced these episodes with clearly lower NO but slightly higher NO_2 concentrations. In this ozone-limited regime, the two deviations have different causes. Whereas the NO deficit has the same causes as in summer, the NO_2 excess contrastingly arises from the partitioning of the increment. With the background ozone nearly exhausted on November 6 and 11, little of the emitted NO can be converted to NO_2, so that the NO_2 share of the increment approaches the effective primary NO_2 fraction of the traffic at the station. The measured increments limit this fraction to about 8 to 9 %, whereas the emission input assumed 20 % for the passenger-car fleet (Section 3.3). The measurements, however, reflect the entire fleet, including buses, heavy-duty and light commercial vehicles, whose share of the NOx emissions and whose primary NO_2 fractions differ from those of passenger cars, so that a car-specific value cannot be expected to match the effective fraction at the station. As the modeled NO_2 share exceeds the measured one by a similar margin on all six days, the NO_2 excess points to the composition of the emitted NOx rather than to its conversion by ozone, and thus to the same input limitation as

the deficit of the NOx increment. A missing chemical pathway would not explain the excess either: an additional VOC-driven conversion of NO into NO_2 would further increase the modeled NO_2. Conversely, the NO_2 share of the measured increment on ozone-limited days offers a way to derive the effective primary NO_2 fraction of a site from routine monitoring data.

4.3 Methodological Limitations and Input Data Constraints

The emission profile generation and simulation boundary conditions relied on several necessary generalizations that introduced inherent uncertainties. While the meteorological wind data were sourced from a proximate, urban-representative monitoring station to capture realistic city-center drag and aerodynamic roughness, minor micro-morphological differences between the station's immediate surroundings and the specific geometry of the Leipziger Straße street canyon, like the missing arcade structures on one street side, may still introduce uncertainties in the initialization of the local atmospheric boundary layer. However, sourcing meteorological data from an urban-representative station rather than an open-field airport station is crucial; previous modeling attempts in similar central Berlin contexts have demonstrated that applying unadjusted open-field wind speeds to inner-city domains leads to excessive mechanical flushing, causing the simulated concentrations to merely mirror background levels and drown out the localized traffic emission signal.

A major limitation for the simulation of NOx lies in the emission inventory itself. The traffic volumes reflect an average-day scenario of passenger cars only, scaled to the official daily count, which enforces a homogeneous fleet without heavy-duty vehicles, buses, and light commercial vehicles. These vehicle classes contribute substantially to the real-world NOx emissions in inner-city streets, and their NOx emissions per vehicle-kilometer are considerably higher than those of passenger cars [5]. In addition, the

uniform emission factor of 0.180 g/km for NOx represents modern passenger cars in fluent traffic, whereas real-world urban driving with frequent acceleration and stop-and-go phases at traffic lights increases the emissions. Both effects lower the modeled local NOx emissions and are consistent with the deficit of the modeled NOx increment, which is largest on November 11 (Section 3.3). The missing vehicle classes also affect the NO/NO_2 partitioning, as the effective primary NO_2 fraction of the mixed fleet differs from the value assumed for passenger cars (Section 4.2). The uniform scaling factor further distributes the emissions inaccurately: while it matches the daily count at the station segment, it overestimates the traffic on neighboring streets, although their contribution at the station is small according to the footprint analysis (Section 4.1).

The local NOx increment is the part of the concentration that local traffic measures can influence, and with a mean measured NO_2 increment of 11 µg/m³ it corresponds to more than half of the annual NO_2 limit value applicable from 2030 (Section 1). The constraints of its simulation identified above stem from the used demonstration dataset rather than from the plugin. The plugin allocates the traffic volume to street segments and hours, and the vehicle fleet enters only through the emission factors and the primary NO_2 fraction. Fleet-average factors for the respective road type, which include the shares of light commercial vehicles, heavy-duty vehicles and buses, can therefore be applied in the same workflow [5, 77], as long as the share of these vehicle classes does not vary strongly over the day. For Berlin, such shares are available per road segment from the official traffic counts [49], and traffic simulations such as SUMO can represent vehicle classes explicitly. Against this background, the 71 % of the measured NOx increment that the model reproduced with passenger cars alone is a lower estimate of what the workflow achieves with a complete fleet description.

An additional process missing from the simulation is the turbulence induced by the moving vehicles themselves, which enhances near-surface mixing and assists the ventilation of the canyon, particularly at low ambient wind speeds. This process is not represented when stationary line sources are used. Including it would further dilute the emitted pollutants at street level. Its absence can therefore not explain the deficit of the modeled NOx increment, which suggests that the emission deficit is, if anything, larger than the increment analysis indicates, but it may contribute to the local overprediction of PM on the most stagnant day.

Finally, potential limitations within the Eulerian framework's capacity to accurately simulate the broad, complex turbulent transport and dispersion of pollutants out of this specific street canyon geometry must also be considered when interpreting the absolute concentration magnitudes. Unmodeled local emission point sources, such as nearby construction sites or side-street traffic leakage, could additionally skew comparisons, alongside highly transient, unrecorded emission events ranging from passing smokers to fugitive emissions [10].

4.4 Study Scope and Proof-of-Concept Robustness

The robustness of the evaluation is constrained by the available observations. Model performance was evaluated against a single observation point at the Leipziger Straße official monitoring station. While this station provides highly accurate data for its specific canyon geometry, relying on one spatial coordinate prevents a comprehensive spatial validation of the broader simulation domain. Furthermore, evaluating the model under only six meteorological scenarios restricts the ability to generalize the workflow's accuracy across a full spectrum of seasonal and synoptic variations.

Despite these limitations, which prevent the study from serving as a validation of the ENVI-met air pollution module, the proof-of-concept shows that the automated workflow produces spatially explicit emission sources whose local signal at the monitoring station captures most of the measured NOx increment, while its timing and partitioning reflect the limitations of the traffic input. For background-dominated pollutants such as PM, the local traffic contribution is better judged by the concentration increment above the background than by the total concentration. The evaluation does not include a comparison with manually created emission input, as the plugin does not alter the emission information itself: the same line sources could be defined by hand in the ENVI-met database. For the present domain, however, this would have required creating 533 line sources with hourly profiles of four species for each of the two seasonal databases, which is impractical and error-prone without automation. The evaluation therefore assesses the emission input generated by the plugin and its interplay with the model rather than the effect of the automation itself.

5 Conclusion

Accurately simulating the dispersion of traffic-related air pollutants at the micro-scale is essential for urban planning and public health assessments, but the application of microclimate models like ENVI-met has been hindered by the manual parameterization of street-level emissions. This study presented an automated method, implemented as an open-source QGIS plugin, that translates traffic trajectory data directly into street-segment-specific ENVI-met emission line sources, together with a procedure to evaluate these sources against monitoring data.

Tested with SUMO trajectories at an official traffic monitoring station in Berlin on six days of contrasting meteorological conditions, the method demonstrated its practical

788 applicability. Combined with the dynamic background concentration forcing of ENVI-
789 met V6, the model reproduced PM concentrations with high agreement and little bias,
790 owed mostly to the regional background that dominates PM at this site. For the reactive
791 gases, passenger-car trajectories alone reproduced 71 % of the measured local NOx
792 increment and the temporal course of NO, while NO was underpredicted on all days,
793 the diurnal maximum of NO_2 was misplaced in summer, and the model assigned a
794 larger share of the NOx increment to NO_2 than observed.

795 The evaluation procedure makes such a comparison with a single monitoring station
796 diagnostic. The background forcing separates the regional from the local contribution,
797 the footprint analysis attributes the local contribution to the emissions of the adjacent
798 street, and the increment of the chemically conserved NOx separates the emitted
799 amount from its chemical partitioning. Along this chain, the remaining deviations were
800 traced mainly to the traffic input of the demonstration, which represents neither the
801 amount nor the composition of the NOx emitted by the real fleet, rather than to the gas-
802 phase chemistry. The procedure thus turns the evaluation into a test of the traffic data
803 themselves and can be transferred to other microscale studies.

804 Despite these input-driven constraints, the presented workflow replaces the manual
805 input and spatial generalization of street-level emissions in micro-scale modeling with
806 an automated, segment-specific procedure, which provides the local increment that
807 matters for exposure assessments and planning scenarios. Future development of the
808 QGIS plugin will focus on accepting diverse traffic trajectory datasets, allowing the
809 explicit parameterization of fleet compositions with class-specific emission factors and
810 primary NO_2 fractions rather than relying solely on passenger-car estimates, and on
811 calibrating the diurnal traffic profiles against local traffic counts. With the emission input
812 automated and post-processing tools like LaStTraM available for source attribution,

subsequent research can readily leverage this tool to conduct comprehensive evaluation studies spanning diverse meteorological conditions and varying urban morphologies. Ultimately, this open-source workflow provides a practical, scalable way of integrating street-segment-specific traffic data into urban microclimate modeling.

Funding

No funding was received for this research.

Ethics, Consent to Participate, and Consent to Publish declarations

Ethics, Consent to Participate, and Consent to Publish declarations: not applicable.

Competing Interest

T. Sinsel and H. Simon act as part-time freelance consultants and software developers for One Click LCA, the company that commercializes the ENVI-met software used in this study.

Data availability

The code of the developed plugin is available in a public GitHub repository (https://github.com/tim-sinsel-jgu-mz/Traffic2ENVI-met) and as package in the QGIS plugin store (https://plugins.qgis.org/plugins/Traffic2ENVImet/). Any further data will be made available on request.

References

1. Lelieveld J, Klingmüller K, Pozzer A, et al (2019) Cardiovascular Disease Burden from Ambient Air Pollution in Europe Reassessed Using Novel Hazard Ratio Functions. European heart journal 40:1590–1596. https://doi.org/10.1093/eurheartj/ehz135

2. Gualtieri M, Ovrevik J, Mollerup S, et al (2011) Airborne Urban Particles (Milan Winter-PM2.5) Cause Mitotic Arrest and Cell Death: Effects on DNA, Mitochondria, AhR Binding and Spindle Organization. Mutation research 713:18–31. https://doi.org/10.1016/j.mrfmmm.2011.05.011

3. Torres-Ramos YD, Montoya-Estrada A, Guzman-Grenfell AM, et al (2011) Urban PM2.5 Induces ROS Generation and RBC Damage in COPD Patients. Frontiers in bioscience (Elite edition) 3:808–817. https://doi.org/10.2741/e288

4. Kampa M, Castanas E (2008) Human health effects of air pollution. Environmental Pollution 151:362–367. https://doi.org/10.1016/j.envpol.2007.06.012

5. European Environment Agency (2025) EMEP/EEA air pollutant emission inventory guidebook 2023 - Update 2025. Passenger cars, light commercial trucks, heavy-duty vehicles including buses, mopeds and motorcycles

6. Karagulian F, Belis CA, Dora CFC, et al (2015) Contributions to Cities' Ambient Particulate Matter (PM): A Systematic Review of Local Source Contributions at Global Level. Atmospheric Environment 120:475–483. https://doi.org/10.1016/j.atmosenv.2015.08.087

7. Minguillón MC, Querol X, Baltensperger U, Prévôt ASH (2012) Fine and coarse PM composition and sources in rural and urban sites in Switzerland: Local or regional pollution? Science of The Total Environment 427–428:191–202. https://doi.org/10.1016/j.scitotenv.2012.04.030

8. Titos G, Lyamani H, Pandolfi M, et al (2014) Identification of fine (PM1) and coarse (PM10-1) sources of particulate matter in an urban environment. Atmospheric Environment 89:593–602. https://doi.org/10.1016/j.atmosenv.2014.03.001

9. Mayer H (1999) Air pollution in cities. Atmospheric Environment 33:4029–4037. https://doi.org/10.1016/S1352-2310(99)00144-2

10. Harr L, Sinsel T, Simon H, et al (2023) Mobile measurements for distribution and attribution of particulate matter in urban environments. Atmospheric Environment 315:120164. https://doi.org/10.1016/j.atmosenv.2023.120164

11. Kumar P, Morawska L, Martani C, et al (2015) The rise of low-cost sensing for managing air pollution in cities. Environment International 75:199–205. https://doi.org/10.1016/j.envint.2014.11.019

12. Britter RE, Hanna SR (2003) FLOW AND DISPERSION IN URBAN AREAS. Annual Review of Fluid Mechanics 35:469–496. https://doi.org/10.1146/annurev.fluid.35.101101.161147

13. Kumar P, Ketzel M, Vardoulakis S, et al (2011) Dynamics and dispersion modelling of nanoparticles from road traffic in the urban atmospheric environment—A review. Journal of Aerosol Science 42:580–603. https://doi.org/10.1016/j.jaerosci.2011.06.001

14. El-Harbawi M (2013) Air quality modelling, simulation, and computational methods: a review. Environ Rev 21:149–179. https://doi.org/10.1139/er-2012-0056

15. Tegen I, Schepanski K, Heinold B (2013) Comparing two years of Saharan dust source activation obtained by regional modelling and satellite observations. Atmospheric Chemistry and Physics 13:2381–2390. https://doi.org/10.5194/acp-13-2381-2013

16. Liu S, Hua S, Wang K, et al (2018) Spatial-temporal variation characteristics of air pollution in Henan of China: Localized emission inventory, WRF/Chem simulations and potential source contribution analysis. Science of The Total Environment 624:396–406. https://doi.org/10.1016/j.scitotenv.2017.12.102

17. Bărbulescu A, Postolache F (2021) New approaches for modeling the regional pollution in Europe. Science of The Total Environment 753:141993. https://doi.org/10.1016/j.scitotenv.2020.141993

18. Im U, Ye Z, Schuhen N, et al (2025) Europe will struggle to meet the new WHO Air Quality Guidelines. npj Clean Air 1:13. https://doi.org/10.1038/s44407-025-00013-w

19. Laudan J, Banzhaf S, Khan B, Nagel K (2024) Coupling MATSim and the PALM Model System—Large Scale Traffic and Emission Modeling with High-Resolution Computational Fluid Dynamics Dispersion Modeling. Atmosphere 15:1183. https://doi.org/10.3390/atmos15101183

20. Laudan J, Banzhaf S, Khan B, Nagel K (2025) Air Quality-Driven Traffic Management Using High-Resolution Urban Climate Modeling Coupled with a Large Traffic Simulation. Atmosphere 16:128. https://doi.org/10.3390/atmos16020128

21. Jänicke B, Milošević D, Manavvi S (2021) Review of User-Friendly Models to Improve the Urban Micro-Climate. Atmosphere 12:1291. https://doi.org/10.3390/atmos12101291

22. Bruse M, Fleer H (1998) Simulating Surface-Plant-Air Interactions inside Urban Environments with a Three Dimensional Numerical Model. Environment Modelling

& Software 13:373–384. https://doi.org/https://doi.org/10.1016/S1364-8152(98)00042-5

23. Bruse M (2022) Particle filtering capacity of urban vegetation: A microscale numerical approach. https://doi.org/10.13140/RG.2.2.23994.56008

24. Heshani ALS, Winijkul E (2022) Numerical simulations of the effects of green infrastructure on PM2.5 dispersion in an urban park in Bangkok, Thailand. Heliyon 8:e10475. https://doi.org/10.1016/j.heliyon.2022.e10475

25. Chen X, He J, Han M, et al (2024) Understanding the impacts of street greening patterns and wind directions on the dispersion of fine particles. Science of The Total Environment 953:176044. https://doi.org/10.1016/j.scitotenv.2024.176044

26. Baradaran Motie M, Yeganeh M, Bemanian M (2023) Assessment of greenery in urban canyons to enhance thermal comfort & air quality in an integrated seasonal model. Applied Geography 151:102861. https://doi.org/10.1016/j.apgeog.2022.102861

27. Du M, Zhao Y, Yang J, et al (2024) Impact of ENVI-met-Based Road Greening Design on Thermal Comfort and PM2.5 Concentration in Hot–Humid Areas. Sustainability 16:8475. https://doi.org/10.3390/su16198475

28. Morakinyo TE, Lam YF (2016) Simulation study of dispersion and removal of particulate matter from traffic by road-side vegetation barrier. Environ Sci Pollut Res 23:6709–6722. https://doi.org/10.1007/s11356-015-5839-y

29. He H, Zhu Y, Liu L, et al (2023) Effects of roadside trees three-dimensional morphology characteristics on traffic-related PM2.5 distribution in hot-humid

925 urban blocks. Urban Climate 49:101448.
926 https://doi.org/10.1016/j.uclim.2023.101448

927 30. Jing L, Liang Y (2021) The impact of tree clusters on air circulation and pollutant
928 diffusion-urban micro scale environmental simulation based on ENVI-met. IOP
929 Conf Ser: Earth Environ Sci 657:012008. https://doi.org/10.1088/1755-
930 1315/657/1/012008

931 31. Deng S, Ma J, Zhang L, et al (2019) Microclimate simulation and model
932 optimization of the effect of roadway green space on atmospheric particulate
933 matter. Environmental Pollution 246:932–944.
934 https://doi.org/10.1016/j.envpol.2018.12.026

935 32. Li L, Zheng M, Zhang J, et al (2023) Effects of green infrastructure on the
936 dispersion of PM2.5 and human exposure on urban roads. Environmental
937 Research 223:115493. https://doi.org/10.1016/j.envres.2023.115493

938 33. Simon H, Fallmann J, Kropp T, et al (2019) Urban Trees and Their Impact on Local
939 Ozone Concentration—A Microclimate Modeling Study. Atmosphere 10:154.
940 https://doi.org/10.3390/atmos10030154

941 34. Harr L, Sinsel T, Simon H, et al (2022) PM2.5 exposure differences between
942 children and adults. Urban Climate 44:101198.
943 https://doi.org/10.1016/j.uclim.2022.101198

944 35. Nikolova I, Janssen S, Vos P, et al (2011) Dispersion Modelling of Traffic Induced
945 Ultrafine Particles in a Street Canyon in Antwerp, Belgium and Comparison with
946 Observations. Science of the Total Environment 412–413:336–343

947 36. Hofman J, Samson R (2014) Biomagnetic monitoring as a validation tool for local
948 air quality models: A case study for an urban street canyon. Environment
949 International 70:50–61. https://doi.org/10.1016/j.envint.2014.05.007

950 37. Paas B, Schneider C (2016) A Comparison of Model Performance between ENVI-
951 met and Austal2000 for Particulate Matter. Atmospheric Environment 145:392–
952 404. https://doi.org/10.1016/j.atmosenv.2016.09.031

953 38. Sun D (Jian), Wu S, Shen S, Xu T (2021) Simulation and assessment of traffic
954 pollutant dispersion at an urban signalized intersection using multiple platforms.
955 Atmospheric Pollution Research 12:101087.
956 https://doi.org/10.1016/j.apr.2021.101087

957 39. ENVI-met by One Click LCA (2026) ENVI-met Release Notes. In: Update History.
958 https://envi-met.info/doku.php?id=apps:updates

959 40. Zhao X, Wu G, Venkatram A, et al (2024) Integrated Simulation Platform for
960 Quantifying the Traffic-Induced Environmental and Health Impacts. In: 2024
961 Forum for Innovative Sustainable Transportation Systems (FISTS). pp 1–8

962 41. San José R, Pérez JL, Gonzalez-Barras RM (2021) Assessment of mesoscale
963 and microscale simulations of a NO2 episode supported by traffic modelling at
964 microscopic level. Science of The Total Environment 752:141992.
965 https://doi.org/10.1016/j.scitotenv.2020.141992

966 42. EU (2024) Directive (EU) 2024/2881 of the European Parliament and of the
967 Council of 23 October 2024 on ambient air quality and cleaner air for Europe
968 (recast)

43. Sinsel T (2026) Plugin GitHub Repository: tim-sinsel-jgu-mz/Traffic2ENVI-met. In: GitHub. https://github.com/tim-sinsel-jgu-mz/Traffic2ENVI-met. Accessed 7 Oct 2026

44. Sinsel T (2026) Traffic Data to ENVI-met - Generates ENVI-met Emission Sources for Model Area and Database based on Traffic Trajectories. In: QGIS Plugins. https://plugins.qgis.org/plugins/Traffic2ENVImet/. Accessed 7 Oct 2026

45. OpenStreetMap (2026) OpenStreetMap. In: Geofabrik Download Server. https://download.geofabrik.de/. Accessed 24 Apr 2026

46. Beamer S, Asanović K, Patterson D (2013) Direction-Optimizing Breadth-First Search. Scientific Programming 21:702694. https://doi.org/10.3233/SPR-130370

47. Simon H (2026) Plugin's GitHub Repository: https://github.com/One-Click-LCA/geodata2ENVI-met. In: GitHub. https://github.com/One-Click-LCA/geodata2ENVI-met. Accessed 24 Sept 2026

48. Berliner Luftgütemessnetz (2026) Stationsdaten: 190 Leipziger Straße | Berliner Luftgütemessnetz, SenMVKU | Luftqualität und Luftgüte in Berlin. https://luftdaten.berlin.de/station/mc190. Accessed 2 Mar 2026

49. GDI Berlin (2019) Daily Traffic Volume 2019 - Leipziger Straße. In: Umweltatlas Berlin - Karten. https://gdi.berlin.de/viewer/umweltatlas/karten/#. Accessed 21 May 2026

50. Ebrahim Shaik Md, Ahmed S (2022) An overview of the impact of COVID-19 on road traffic safety and travel behavior. Transportation Engineering 9:100119. https://doi.org/10.1016/j.treng.2022.100119

51. Kirchner I, Gebauer P, Langer I, et al (2025) Meteorologische Messungen im Berliner Stadtgebiet mit MEVIS Stationen des Instituts für Meteorologie der Freien Universität Berlin für das Jahr 2024

52. World Meteorological Organization (WMO) (2024) Guide to Instruments and Methods of Observation, 8th ed

53. MEVIS Support Team at IfM (2025) MEVIS Dokumentation Station: 21_Moabit-1. Institut für Meteorologie, Freie Universität Berlin, Berlin

54. Ouyang W, Morakinyo TE, Ren C, et al (2021) Thermal-Irradiant Performance of Green Infrastructure Typologies: Field Measurement Study in a Subtropical Climate City. Science of The Total Environment 764:144635. https://doi.org/10.1016/j.scitotenv.2020.144635

55. Liu Z, Cheng W, Jim CY, et al (2021) Heat Mitigation Benefits of Urban Green and Blue Infrastructures: A Systematic Review of Modeling Techniques, Validation and Scenario Simulation in ENVI-met V4. Building and Environment 200:107939. https://doi.org/10.1016/j.buildenv.2021.107939

56. Schöneberger P, Sinsel T, Ouyang W, et al (2025) Enhancing urban microclimate simulations: Validating ENVI-met's accuracy in modeling multi-directional radiative fluxes and mean radiant temperature in subtropical hong kong. Building and Environment 284:113475. https://doi.org/10.1016/j.buildenv.2025.113475

57. Berliner Luftgütemessnetz (2026) Stationsdaten: 010 Wedding | Berliner Luftgütemessnetz, SenMVKU | Luftqualität und Luftgüte in Berlin. https://luftdaten.berlin.de/station/mc010. Accessed 22 Apr 2026

58. Berliner Luftgütemessnetz (2026) Stationsdaten: 042 Neukölln | Berliner Luftgütemessnetz, SenMVKU | Luftqualität und Luftgüte in Berlin. https://luftdaten.berlin.de/station/mc042. Accessed 4 Aug 2026

59. Berliner Luftgütemessnetz (2026) Stationsdaten: 171 Mitte | Berliner Luftgütemessnetz, SenMVKU | Luftqualität und Luftgüte in Berlin. https://luftdaten.berlin.de/station/mc171. Accessed 4 Aug 2026

60. Trebs I, Bohn B, Ammann C, et al (2009) Relationship between the NO_2 photolysis frequency and the solar global irradiance. Atmospheric Measurement Techniques 2:725–739. https://doi.org/10.5194/amt-2-725-2009

61. Koepke P, Garhammer M, Hess M, Roeth E-P (2010) NO_2 photolysis frequencies in street canyons. Atmospheric Chemistry and Physics 10:7457–7466. https://doi.org/10.5194/acp-10-7457-2010

62. Lopez PA, Behrisch M, Bieker-Walz L, et al (2018) Microscopic Traffic Simulation using SUMO. In: 2018 21st International Conference on Intelligent Transportation Systems (ITSC). pp 2575–2582

63. Schrab K, Protzmann R, Radusch I (2023) A Large-Scale Traffic Scenario of Berlin for Evaluating Smart Mobility Applications. In: Nathanail EG, Gavanas N, Adamos G (eds) Smart Energy for Smart Transport. Springer Nature Switzerland, Cham, pp 276–287

64. Ziemke D, Kaddoura I, Nagel K (2019) The MATSim Open Berlin Scenario: A multimodal agent-based transport simulation scenario based on synthetic demand modeling and open data. Procedia Computer Science 151:870–877. https://doi.org/10.1016/j.procs.2019.04.120

65. Simon H, Heusinger J, Sinsel T, et al (2021) Implementation of a Lagrangian Stochastic Particle Trajectory Model (LaStTraM) to Simulate Concentration and Flux Footprints Using the Microclimate Model ENVI-Met. Atmosphere 12:977. https://doi.org/10.3390/atmos12080977

66. Simon H, Sinsel T (2026) LaSTraM Binary Download

67. Hanna S, Chang J (2012) Acceptance criteria for urban dispersion model evaluation. Meteorol Atmos Phys 116:133–146. https://doi.org/10.1007/s00703-011-0177-1

68. Kljun N, Rotach MW, Schmid HP (2002) A Three-Dimensional Backward Lagrangian Footprint Model for a Wide Range of Boundary-Layer Stratifications. Boundary-Layer Meteorology 103:205–226. https://doi.org/10.1023/a:1014556300021

69. Markkanen T, Steinfeld G, Kljun N, et al (2009) Comparison of Conventional Lagrangian Stochastic Footprint Models against LES Driven Footprint Estimates. Atmospheric Chemistry and Physics 9:5575–5586. https://doi.org/10.5194/acp-9-5575-2009

70. Hellsten A, Luukkonen S-M, Steinfeld G, et al (2015) Footprint Evaluation for Flux and Concentration Measurements for an Urban-Like Canopy with Coupled Lagrangian Stochastic and Large-Eddy Simulation Models. Boundary-Layer Meteorology 157:191–217. https://doi.org/10.1007/s10546-015-0062-4

71. Weil JC, Sullivan PP, Moeng C-H (2004) The Use of Large-Eddy Simulations in Lagrangian Particle Dispersion Models. Journal of the Atmospheric Sciences 61:2877–2887. https://doi.org/10.1175/jas-3302.1

72. Maronga B, Gryschka M, Heinze R, et al (2015) The Parallelized Large-Eddy Simulation Model (PALM) Version 4.0 for Atmospheric and Oceanic Flows: Model Formulation, Recent Developments, and Future Perspectives. Geoscientific Model Development 8:2515–2551. https://doi.org/10.5194/gmd-8-2515-2015

73. Kim S, Kim NG, Kim J, et al (2024) Impact of vehicles at the roadside of expressway in urban area: Simultaneous measurement of particle size distribution and positive matrix factorization. Science of The Total Environment 949:175051. https://doi.org/10.1016/j.scitotenv.2024.175051

74. Wu X, Vu TV, Harrison RM, et al (2022) Long-term characterization of roadside air pollutants in urban Beijing and associated public health implications. Environmental Research 212:113277. https://doi.org/10.1016/j.envres.2022.113277

75. Maher BA, Gonet T, Karloukovski VV, et al (2022) Protecting playgrounds: local-scale reduction of airborne particulate matter concentrations through particulate deposition on roadside ‘tredges’ (green infrastructure). Sci Rep 12:14236. https://doi.org/10.1038/s41598-022-18509-w

76. Bright VB, Bloss WJ, Cai X (2013) Urban street canyons: Coupling dynamics, chemistry and within-canyon chemical processing of emissions. Atmospheric Environment 68:127–142. https://doi.org/10.1016/j.atmosenv.2012.10.056

77. Environmental Protection Agency of Germany (2017) The Handbook of Emission Factors for Road Transport (HBEFA)